Effect of pH on the Nitrite Hydrogenation Mechanism over Pd/Al_2O_3 and Pt/Al_2O_3: Details Obtained with ATR-IR Spectroscopy†

Sune D. Ebbesen,‡ Barbara L. Mojet, and Leon Lefferts*

Catalytic Processes and Materials, Faculty of Science and Technology, Institute of Mechanics Processes and Control Twente (IMPACT) and MESA+ Institute for Nanotechnology, University of Twente, P.O. Box 217, 7500 AE Enschede, The Netherlands

Received: July 14, 2010; Revised Manuscript Received: November 15, 2010

It is well-known that activity and selectivity to N_2 during nitrite hydrogenation over noble metal catalysts in water depend on the pH of the solution, but mechanistic understanding is lacking. Attenuated total reflection infrared (ATR-IR) spectroscopy is an ideal tool to perform detailed studies on catalytic surfaces in water. In this paper, the influence of pH was studied on adsorption and subsequent hydrogenation of nitrite in water between pH 5 and 9 over Pd/Al_2O_3 and Pt/Al_2O_3, using ATR-IR spectroscopy. On both catalysts, pH clearly influenced the surface coverage and reaction rates of intermediates. For Pt/Al_2O_3, lowering the pH induced the increasing surface coverage of key reaction intermediates like $NO_{steps}^{1620\ cm^{-1}}$ and "HNO"$_{(ads)}^{1540\ cm^{-1}}$, as well as increased hydrogenation rates, explaining the higher TOF at lower pH as reported in the literature. For Pd/Al_2O_3, the effect of pH on selectivity is controlled by the rate constants of the formation and hydrogenation of the most stable reaction intermediates to N_2 ($NO_{(ads)}^{1720\ cm^{-1}}$) and NH_4^+ ($NH_{2(ads)}^{1510\ cm^{-1}}$).

Introduction

Increasing nitrite and nitrate levels in groundwater cause environmental concerns, and increasingly strict water quality regulations require removal of nitrite and nitrate from groundwater.[1] The most promising method for nitrate and nitrite removal is based on selective hydrogenation over noble metal catalysts, which was first described in 1989.[2] Since then, the catalytic hydrogenation of nitrite and nitrate for use in water purification has been examined extensively.[3−14] Nitrite hydrogenation can be performed over single noble metal catalysts such as platinum and palladium catalysts, where palladium catalysts show a higher selectivity to nitrogen, with ammonia as the side product. High selectivity toward nitrogen is desirable, since ammonia is toxic as well. Both pH and hydrogen concentration were found to influence the selectivity toward nitrogen and ammonia. At high hydrogen concentration, the main product is ammonia,[6,15,16] whereas the highest selectivity to nitrogen is found at low pH.[2,4,5,7,11]

We have recently investigated the adsorption of reactants and intermediates on the catalyst surface during hydrogenation of nitrite over Pd/Al_2O_3 and Pt/Al_2O_3 at pH 7 by attenuated total reflection infrared spectroscopy (ATR-IR).[3,10,12,17] Scheme 1 shows the proposed hydrogenation mechanisms of nitrite over Pd/Al_2O_3 and Pt/Al_2O_3. On Pd/Al_2O_3, two important surface intermediates were detected: $NH_{2(ads)}$ and $NO_{(ads)}$. It was shown that $NH_{2(ads)}$ is converted to ammonia solely. In contrast, $NO_{(ads)}$ is converted to a reaction product that is not infrared active, suggesting nitrogen as the possible reaction product. For Pt/Al_2O_3, the reaction proceeds via a similar stepwise hydrogenation process, except that in this case also cross-reactions are possible between the two paths to the main products N_2 and ammonia. Over Pt/Al_2O_3, $NO_{(ads)}$ is hydrogenated to both nitrogen and ammonia,[3] similar to electroreduction of nitrite/NO adlayers.[18−23] Further, hydrogenation of nitrite over platinum is structure sensitive; on platinum, the NO intermediate was found to adsorb on low index surfaces ($NO_{(ads)}^{1580\ cm^{-1}}$) as well as to accumulate on steps ($NO_{(steps)}^{1620\ cm^{-1}}$),[3] as also observed during electrochemical reduction of nitrate over platinum electrodes.[24]

It is well-known that activity and selectivity to N_2 during nitrite hydrogenation depend on the pH of the solution.[2,4,5,7,11] However, the mechanistic reason for this activity and selectivity pattern has not been investigated in detail yet. It is the aim of this study to examine the influence of pH on the adsorbed

SCHEME 1: Proposed Reaction Pathways for Nitrite Hydrogenation over Pd/Al_2O_3 (left) and Pt/Al_2O_3 (right)[3,10] *a*

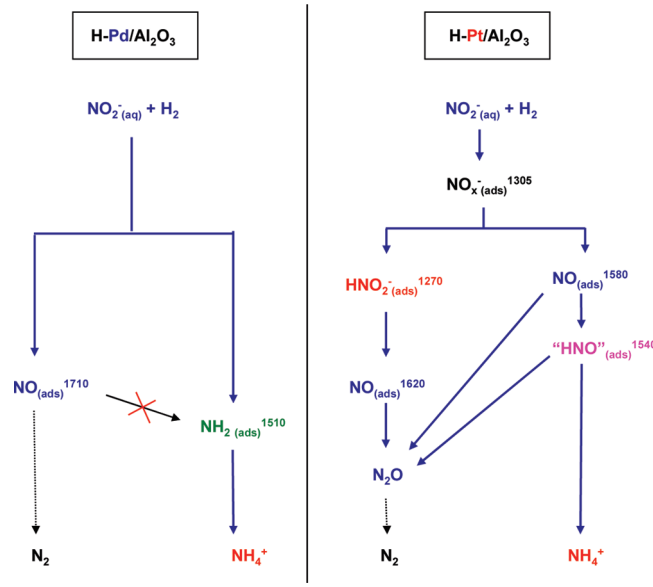

a The dotted lines represent proposed reaction pathways for N_2 formation.

† Part of the "Alfons Baiker Festschrift".

* Corresponding author. Phone: +31 53 489 2858. Fax: +31 53 489 4683. E-mail: L.Lefferts@utwente.nl.

‡ Present address: Fuel Cells and Solid State Chemistry Division, Risø National Laboratory, Denmark.

10.1021/jp106521t
Published on Web 12/02/2010

species during hydrogenation of nitrite in water with pH between 5 and 9 over Pd/Al_2O_3 and Pt/Al_2O_3 using ATR-IR spectroscopy.

Experimental Section

Catalyst Preparation. A 5 wt % Pt/Al_2O_3 powder catalyst was prepared and characterized as previously described.[3,12] In short, precalcined γ-Al_2O_3 powder was impregnated with a solution of $H_2PtCl_6 \cdot 6H_2O$ (Alfa Aesar) to yield a catalyst with 5 wt % platinum loading.[3,17] The slurry was mixed for 2 h, followed by drying at 335 K for 2 h in a rotating evaporator. The impregnated Pt/Al_2O_3 powder was then calcined at 673 K for 3 h (heating rate 5 K/min) in synthetic air (30 mL/min) and reduced at 673 K for 3 h (heating rate 5 K/min) in hydrogen (30 mL/min).

The Pd/Al_2O_3 catalyst was prepared from adsorption of palladium acetylacetonate ($Pd(acac)_2$) (Alfa Aesar) onto γ-Al_2O_3 powder to yield a catalyst with a 5 wt % palladium loading.[12] The mixture was filtered and dried at 323 K for 15 h in stagnant air, followed by calcination at 573 K (heating/cooling rate 1 K/min) in synthetic air (30 mL/min). In order to obtain a metal loading of 5 wt % palladium, this procedure was repeated five times with the remaining filtrate from the first ion exchange. Subsequently, the calcined catalyst was reduced at 323 K for 2 h (heating/cooling rate 1 K/min) in hydrogen (30 mL/min), followed by flushing with argon (30 mL/min) at 600 K for 1 h (heating/cooling rate 1 K/min) to avoid the formation of any palladium hydride.

Preparation of Thin Catalyst Layers on the Internal Reflection Element. Subsequently, each of the catalyst powders was deposited on a ATR-IR ZnSe internal reflection element (IRE) and mounted in an *in situ* ATR-IR cell as previously described.[3,10,12,17] A suspension of either Pd/Al_2O_3 or Pt/Al_2O_3 was prepared in water; the pH was adjusted to 3.5 with nitric acid to stabilize small alumina particles. The suspension was milled for 1 h in a ball-mill (Fritsch Pulverisette) to obtain particles of a few nanometers in size as determined by SEM. Subsequently, colloidal alumina corresponding to 5 wt % of the catalyst amount was added (aluminum oxide, 20% in H_2O colloidal suspension, Alfa Aesar, particle size 5 nm). The catalyst layer was prepared on the IRE by adding the catalyst/water suspension evenly on one side of the IRE. Each catalyst layer was prepared on a ZnSe IRE by adding 1 mL of the catalyst/water suspension evenly on one side of the IRE. The suspension was allowed to evaporate overnight at room temperature. Subsequently, the catalyst layer/IRE was heated to 573 K for 2 h (heating rate 1 K/min) in flowing argon to ensure removal of all NO_x species on the catalyst surface. The deposition procedure had to be repeated once for the Pd/Al_2O_3 layer, in order to limit the formation of cracks in the final catalyst layer. About 6 mg of catalyst was deposited on the IRE in all cases. Further, an additional reduction treatment was necessary for Pt/Al_2O_3 in order to remove all NO_x species (heating to 673 K in hydrogen, heating/cooling rate 10 K/min). For Pt/Al_2O_3, the platinum dispersion was measured for the powder catalyst using hydrogen chemisorption to 75%, resulting in 0.192 mmol of accessible platinum surface atoms when prepared on the IRE. The thickness of the Pt/Al_2O_3 catalyst layer was 3.50 ± 0.25 μm. For Pd/Al_2O_3, the metal dispersion was 45% as determined with CO chemisorption assuming CO:Pd = 1, resulting in 0.206 mmol of accessible metal surface atoms for the catalyst layer on the IRE.[12] The thickness of the Pd/Al_2O_3 catalyst layer was 5.0 ± 0.5 μm.[17,25]

***In Situ* ATR-IR Spectroscopy.** The water used in all ATR-IR experiments was ultrapure Q2-water prepared with a Millipore Milli-Q water treatment system from Amphotech Ltd. Saturation of water with Ar (5.0, Praxair), or H_2 (5.0, Praxair), was performed at room temperature (294 K) with gas flow rates of 40 mL$\cdot$min^{-1} for a minimum of 2 h. Prior to saturation with H_2, air was removed by saturation with argon for at least 2 days. The concentrations of dissolved gases in water were calculated on the basis of reported solubility data at room temperature and 1 atm of gas pressure resulting in 2.3×10^{-3} mol$\cdot$L^{-1} Ar/H_2O and 4.1×10^{-4} mol$\cdot$L^{-1} H_2/H_2O.[26]

The hydrogenation experiments were carried out with much lower H_2 concentration (4.1×10^{-6} mol$\cdot$L^{-1} H_2/H_2O, saturated at 0.001 bar of H_2) to slow down reaction rates.

A solution of $NO_2^-{}_{(aq)}$ (4.3×10^{-4} mol$\cdot$L^{-1}) was prepared in Ar/H_2O from $NaNO_2$ (Merck). For all liquids, the pH was adjusted by adding NaOH (Merck) or HCl (37% Merck); pH was measured using a pH meter (744 pH meter, Metrohm).

ATR-IR spectra were recorded using a home-built stainless steel flow-through cell as described elsewhere.[27] All ATR-IR spectra were recorded at room temperature (294 K) in an air-conditioned room. Infrared spectra were recorded by averaging of 128 scans with a resolution of 4 cm^{-1}, which took about 78 s. This is approximately 10 times longer than the liquid residence time in the cell. Thus, each spectrum represents the overall changes in the spectra over a period of about 78 s. The interval between the start of two subsequent spectra was 90 s. The ATR-IR cell was assembled with the coated IRE and mounted in the sample compartment of the infrared spectrometer. Hereafter, the sample compartment was flushed with nitrogen, and the cell was flushed with either Ar/H_2O or reduced *in situ* by introducing H_2/H_2O. The catalysts are denoted Pt/Al_2O_3 and Pd/Al_2O_3 when treated with Ar/H_2O and H$-$$Pt/Al_2O_3$ and H$-$$Pd/Al_2O_3$ when treated with H_2/H_2O.

Data Treatment. As shown previously, the ATR-IR spectra must be corrected for the infrared absorbance of water by subtracting a scaled ATR-IR spectrum of water.[27] To calculate the respective peak areas, curve fitting was applied after subtraction of the water spectra. Curve fitting was performed using a Lorentzian function. The applied Lorentzian line-shape function centered at the frequency ω_0 is $I(\omega) = A \cdot (2/\pi) \cdot \{w/[4 \cdot (\omega - \omega_0) + w^2]\}$, where $I(\omega)$ is the intensity at a given frequency ω, A is the integrated peak area, and w is the full width at half of the maximum intensity.

Results

Pd/Al_2O_3. Adsorption of $NO_2^-{}_{(aq)}$ on Passivated Pd/Al_2O_3. After assembling the ATR-IR cell with a Pd/Al_2O_3 coated IRE, the cell was flushed with Ar/H_2O at pH values corresponding to the subsequent experiments. After flushing, a solution of 4.3×10^{-4} mol/L $NO_2^-{}_{(aq)}$ was introduced to the cell at the same pH. Figure 1a shows ATR-IR spectra obtained after adsorption of $NO_2^-{}_{(aq)}$ on Pd/Al_2O_3 at pH 5.2$-$9.1, and the corresponding integrated peak areas are given in Figure 1b. After each adsorption experiment, the cell was dismantled and the catalyst/IRE was reduced *ex situ* at 573 K and cooled to room temperature in argon, to make sure any adsorbed species are completely removed before using the same catalyst layer again for the next experiment. In this way, the same catalyst layer was used for all adsorption studies, which is particularly important, since this allows comparison of intensities between different adsorption experiments. The adsorption experiments were performed in random order and could be reproduced, showing that the layer was thermally stable during *ex situ* reduction.

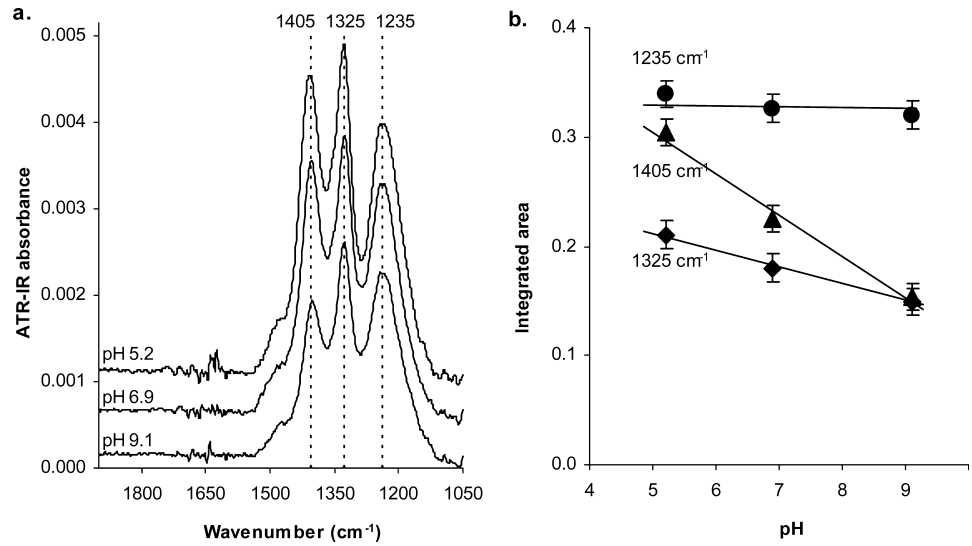

Figure 1. (a) Water corrected ATR-IR spectra while a solution of $NO_2^-{}_{(aq)}$ was flown over Pd/Al_2O_3 at pH 5.2, 6.9, and 9.1. (b) Corresponding integrated peak areas.

During flow of $NO_2^-{}_{(aq)}$ over Pd/Al_2O_3, infrared peaks evolved at 1405, 1325, and 1235 cm^{-1} (Figure 1). Further, a shoulder was observed at 1475 cm^{-1}. These results are similar to results obtained at neutral pH, where $NO_x^-{}_{(ads,\ x=2,3)}$ on palladium was observed at 1475, 1405, and 1325 cm^{-1}.[10] It is well-known that nitrite can adsorb in different geometries, which can be divided into two main categories: nitro (coordinated via the nitrogen atom) and nitrito (coordinated by one or two of the oxygen atoms). All of these species have N−O stretch frequencies reported between 1500 and 1200 cm^{-1}; however, there is significant disagreement in the literature concerning the exact assignment.[28] Moreover, infrared frequencies for nitrate species have been reported in the same range. Since the experiments were performed on catalyst surfaces that were passivated during transport through air, formation of surface nitrates cannot be excluded at this point. Furthermore, the high dispersion of the metal particles indicates that many different crystal planes, steps, and kinks will be present, which provide a variety of metal adsorption sites. From single crystal studies, it is well-known that each type of adsorption site gives rise to unique metal-adsorbate vibrational properties.

The peak at 1235 cm^{-1} indicates the presence of $NO_2^-{}_{(aq)}$.[12] Figure 1 shows that, while the intensity of $NO_2^-{}_{(aq)}$ is constant within the experimental error with changing pH, the intensity of both adsorbed $NO_x^-{}_{(ads)}$ species clearly lowered with increasing pH. Further, also the integrated intensity ratio of $NO_x^{-1405\ cm^{-1}}{}_{(ads)}$/ $NO_x^{-1325\ cm^{-1}}{}_{(ads)}$ decreased with increasing pH, confirming that the two peaks are due to two differently adsorbed $NO_x^-{}_{(ads)}$ species.

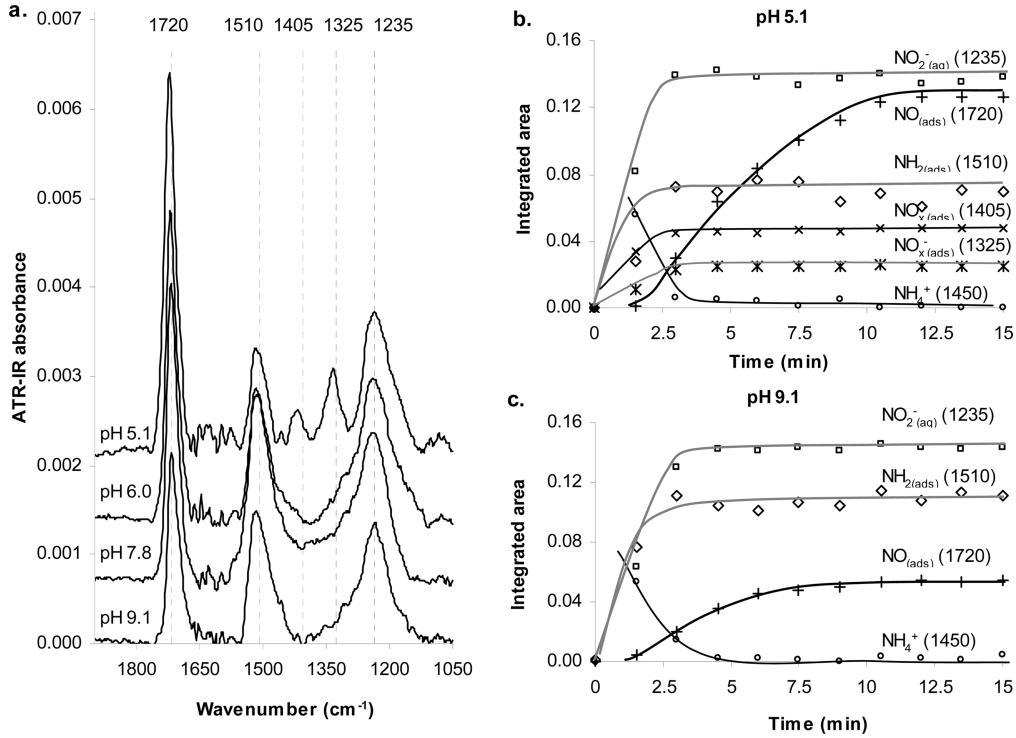

Figure 2. (a) Water corrected ATR-IR spectra after adsorption of $NO_2^-{}_{(aq)}$ on $H-Pd/Al_2O_3$ for 15 min at pH 5.1, 6.0, 7.8, and 9.1. (b and c) Integrated peak areas during adsorption of nitrite over $H-Pd/Al_2O_3$ at pH 5.1 (b) and pH 9.1 (c).

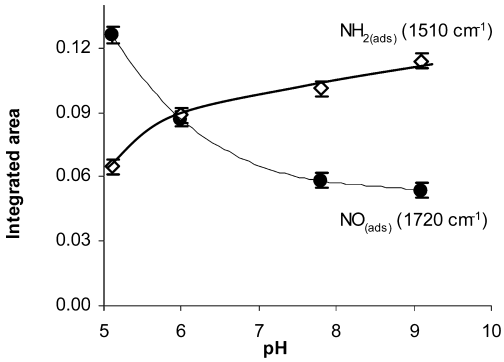

Figure 3. Final integrated peak areas of $NH_{2(ads)}$ and $NO_{(ads)}$ after adsorption of nitrite for 15 min on H−Pd/Al_2O_3 as a function of pH.

Adsorption of $NO_2^-{}_{(aq)}$ on Reduced H−Pd/Al_2O_3. After assembling the ATR-IR cell with a Pd/Al_2O_3 coated IRE, the catalyst was reduced *in situ* at pH 5.1, 6.0, 7.8, and 9.1. After reduction, the cell was flushed with Ar/H_2O while the pH was kept the same as during reduction. Subsequently, $NO_2^-{}_{(aq)}$ was flown through the cell, again at the same pH. Figure 2a shows the ATR-IR spectra obtained after 15 min of adsorption of $NO_2^-{}_{(aq)}$ on H−Pd/Al_2O_3 at pH 5.2−9.1. The observed peaks have previously been assigned to the following species: $NO_2^-{}_{(aq)}$ (1235 cm^{-1}), $NO_x^-{}_{(ads,\ x=2,3)}$ (1405 and 1325 cm^{-1}), NH_4^+ (1450 cm^{-1}), $NO_{(ads)}$ (1720 cm^{-1}), and $NH_{2(ads)}$ (1510 cm^{-1}).[12] Figure 2a shows that exclusively at pH 5.1 NO_x^- adsorbed on palladium was detected at 1405 and 1325 cm^{-1}.

The integrated areas of the peaks during the first 15 min of adsorption of $NO_2^-{}_{(aq)}$ on H−Pd/Al_2O_3 are shown in Figure 2b and c at, respectively, the lowest pH (5.1) and highest pH (9.1) investigated. It can be seen that the intensity of the observed infrared peaks stabilized within 15 min.

Initially, $NH_{2(ads)}^{1510\ cm^{-1}}$ and $NH_4^{+\ 1450\ cm^{-1}}$ formed on the catalyst surface followed by formation of $NO_{(ads)}^{1720\ cm^{-1}}$, similar to the experiments at neutral pH as previously published.[10] Moreover, the formation of $NO_{(ads)}^{1720\ cm^{-1}}$ is retarded at all pH values investigated. Further, the exact final peak position of the species $NO_{(ads)}^{1720\ cm^{-1}}$ shifts from 1723 to 1721 to 1719 and finally to 1717 cm^{-1} with pH changing from 5.1 to 9.1. The final intensities of $NH_{2(ads)}^{1510\ cm^{-1}}$ and $NO_{(ads)}^{1720\ cm^{-1}}$ are plotted in Figure 3. Clearly, the amount of $NH_{2(ads)}^{1510\ cm^{-1}}$ increases while the amount $NO_{(ads)}^{1720\ cm^{-1}}$ decreases with higher pH.

Hydrogenation of $NO_x^-{}_{(ads)}$, $NO_{(ads)}$, and $NH_{2(ads)}$ on Pd/Al_2O_3. After adsorbing $NO_2^-{}_{(aq)}$ on H−Pd/Al_2O_3, as described above, the cell was flushed with Ar/H_2O at the same pH applied during adsorption. While flushing, all adsorbed species appeared stable, whereas $NO_2^-{}_{(aq)}$ was flushed out of the cell immediately. Subsequently, H_2/H_2O at the same pH was introduced to hydrogenate the adsorbed species. As a typical example, the ATR-IR spectra during hydrogenation at pH 5.1 and the integrated intensity of the adsorbed species are shown in Figure 4.

The results in Figure 4 are typical for all experiments on Pd/Al_2O_3 performed at different pH, although with different intensities of the adsorbed species. As said above, only at pH 5.1 $NO_x^-{}_{(ads,\ x=2,3)}$ (1405 and 1325 cm^{-1}) was observed, which quickly disappeared after hydrogen was introduced. $NO_{(ads)}^{1720\ cm^{-1}}$ was the first species to disappear during the hydrogenation, while the intensity $NH_{2(ads)}^{1510\ cm^{-1}}$ was constant within the experimental error. During hydrogenation of $NO_{(ads)}^{1720\ cm^{-1}}$, the peak shifted to lower wavenumber due to diminishing dipole−dipole interactions.[10] Only after a while, $NH_{2(ads)}^{1510\ cm^{-1}}$started to decrease and at the same time $NH_4^{+\ 1450\ cm^{-1}}$ appeared. Removal of $NH_{2(ads)}^{1510\ cm^{-1}}$ started approximately at 11−12 min in all cases, typically once the intensity for $NO_{(ads)}^{1720\ cm^{-1}}$ had decreased to about 30−40% of the initial intensity, independent of pH.

Figure 5 shows the removal of $NO_{(ads)}^{1720\ cm^{-1}}$ and $NH_{2(ads)}^{1510\ cm^{-1}}$ at different pH values as a function of time. It is observed that all adsorbed $NO_{(ads)}^{1720\ cm^{-1}}$ has disappeared after approximately the same time, i.e., 25 min, independent of pH and initial intensity. For $NH_{2(ads)}^{1510\ cm^{-1}}$, the situation is completely different (Figure 5b). At pH 9.1, $NH_{2(ads)}^{1510\ cm^{-1}}$ has the highest intensity but disappears the fastest (within 24 min), while, at pH 5.1, the intensity of $NH_{2(ads)}^{1510\ cm^{-1}}$ is initially the lowest but the species disappears the slowest.

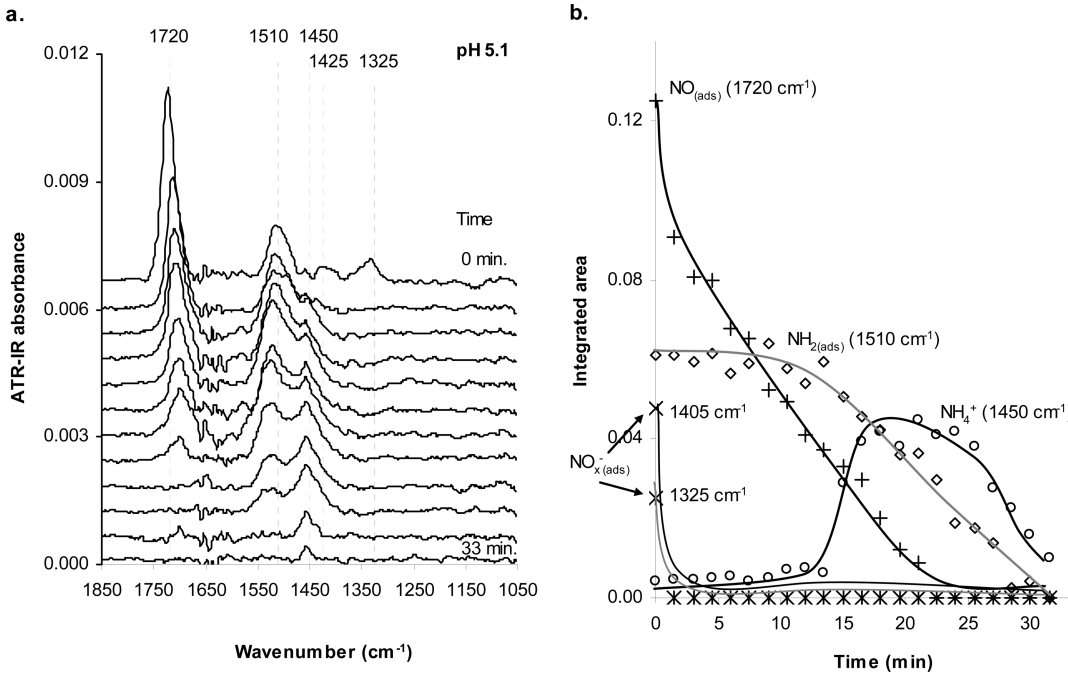

Figure 4. (a) Water corrected ATR-IR spectra during hydrogenation of $NO_{(ads)}$, $NH_{2(ads)}$, and $NO_x^-{}_{(ads)}$ on Pd/Al_2O_3, formed on the catalyst surface during adsorption of $NO_2^-{}_{(aq)}$ on H−Pd/Al_2O_3 at pH 5.1. (b) Corresponding integrated peak intensities during hydrogenation.

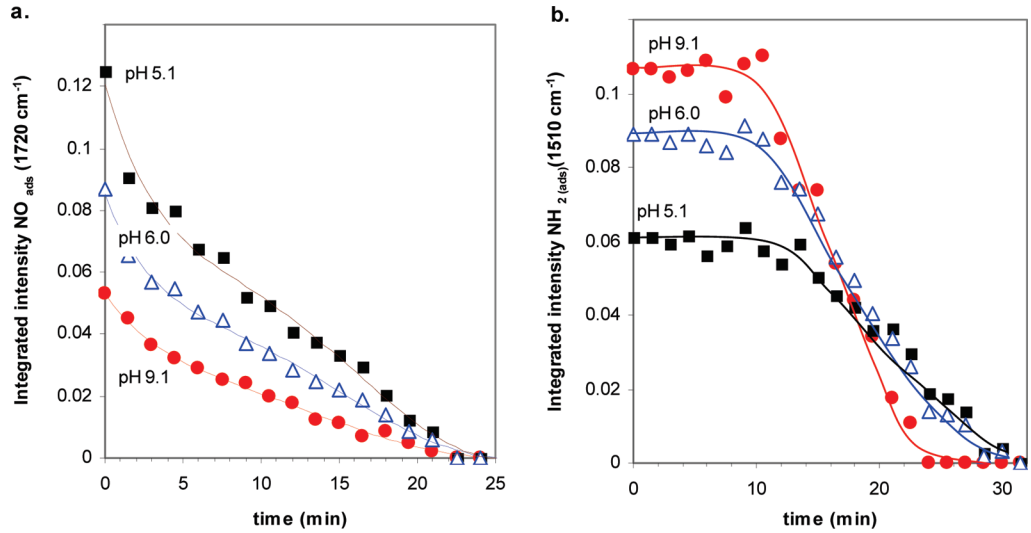

Figure 5. Removal of (a) $NO_{(ads)}^{1720\ cm^{-1}}$ and (b) $NH_{2(ads)}^{1510\ cm^{-1}}$ on Pd/Al_2O_3 as a function of pH. Data at pH 7.8 have been omitted for clarity. pH 5.1, closed squares; pH 6.0, open triangles; pH 9.1, closed circles.

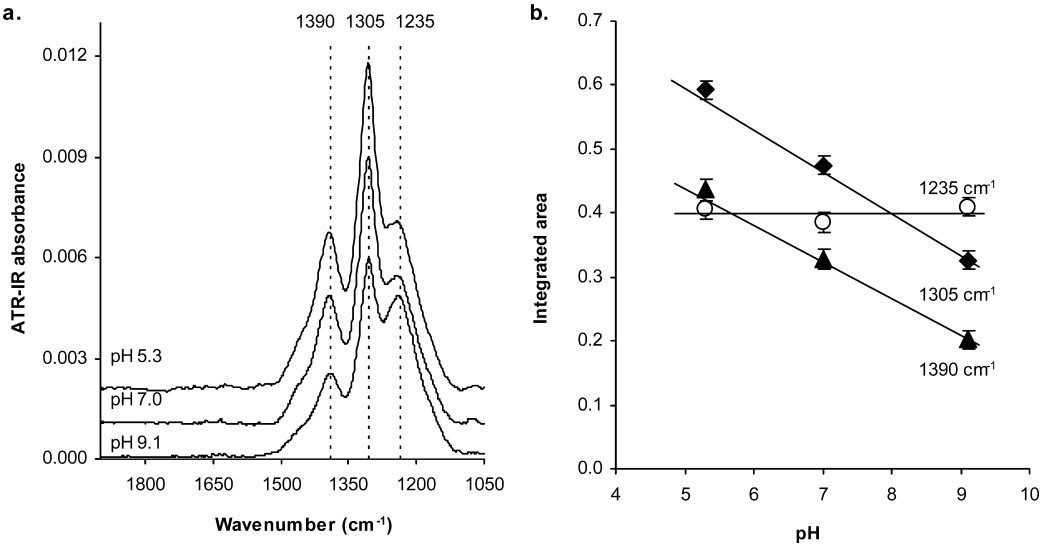

Figure 6. (a) Water corrected ATR-IR spectra while a solution of $NO_2^-{}_{(aq)}$ was flown over Pt/Al_2O_3 at pH 5.3, 7.0, and 9.1. (b) Corresponding integrated peak areas.

Pt/Al_2O_3. *Adsorption of $NO_2^-{}_{(aq)}$ on Passivated Pt/Al_2O_3.* After assembling the ATR-IR cell with a Pt/Al_2O_3 coated IRE, the cell was flushed with Ar/H_2O at pH values corresponding to the subsequent experiments, similar to the procedure for adsorbing $NO_2^-{}_{(aq)}$ on Pd/Al_2O_3 described above. Subsequently, $NO_2^-{}_{(aq)}$ was flown through the cell at the corresponding pH. Figure 6a shows ATR-IR spectra obtained after adsorption of $NO_2^-{}_{(aq)}$ on Pt/Al_2O_3 at pH 5.3−9, and Figure 6b shows the corresponding integrated peak areas.

During flow of $NO_2^-{}_{(aq)}$ over Pt/Al_2O_3, infrared peaks were observed at 1390, 1305, and 1235 cm^{-1} and the peak positions were independent of pH; the intensities stabilized completely after 15 min. (Note: the apparent small shift of the peak at 1235 cm^{-1} in Figure 6 is due to the overlap with the peak at 1305 cm^{-1}, and does not reflect a shift in frequency of the vibration, as determined by the curve fitting procedure described in the Experimental Section.) In a previous paper, we have shown that adsorption of $NO_2^-{}_{(aq)}$ (at 1235 cm^{-1}) on passivated platinum leads to two different adsorbed NO_x species on the platinum surface, observed at, respectively, 1390 and 1305 cm^{-1};[12] these peaks are denoted $NO_x^{-1305\ cm^{-1}}{}_{(ads)}$ and $NO_x^{-1390\ cm^{-1}}{}_{(ads)}$ in the following. Figure 6b clearly shows that the integrated peak intensities of both $NO_x^-{}_{(ads)}$ species decreased with increasing pH, while the intensity of dissolved $NO_2^-{}_{(aq)}$ remained constant.

Adsorption of $NO_2^-{}_{(aq)}$ on H−Pt/Al_2O_3. As for Pd/Al_2O_3, the Pt/Al_2O_3 catalyst was reduced *in situ* in water at the required pH (denoted H−Pt/Al_2O_3) and subsequently the cell was flushed with Ar/H_2O at the same pH as applied during reduction. After reduction, $NO_2^-{}_{(aq)}$ with the corresponding pH was introduced into the cell. Figure 7a shows ATR-IR spectra obtained after adsorption of $NO_2^-{}_{(aq)}$ on H−Pt/Al_2O_3 at pH 5.3−9.1 for 15 min. The development of the integrated peak areas at pH 5.3 and 9.1 is shown in Figure 7b and c.

As shown in Figure 7, infrared peaks were observed at 2231, 1580, 1540, 1455, 1390, 1305, and 1235 cm^{-1}, which are assigned to $N_2O^{2231\ cm^{-1}}$, $NO_{ads}^{1580\ cm^{-1}}$, "$HNO"_{(ads)}^{1540\ cm^{-1}}$, $NH_4^{+\ 1455\ cm^{-1}}$, $NO_x^{-1390\ cm^{-1}}{}_{(ads)}$, $NO_x^{-1305\ cm^{-1}}{}_{(ads)}$, and $NO_2^-{}_{(aq)}$ (1235 cm^{-1}), respectively, as previously discussed for the experiment performed at pH 7.0.[3] From Figure 7, it can be seen that the same surface intermediates are formed on the platinum surface at all investigated pH values, though some with different intensities (Figure 7b and c). The final peak intensities of $NO_2^-{}_{(aq)}$ (1235 cm^{-1}), $NO_x^{-1390\ cm^{-1}}{}_{(ads)}$, $NH_4^{+\ 1455\ cm^{-1}}$, and "$HNO"_{(ads)}^{1540\ cm^{-1}}$ were constant, independent of pH. The intensities for $NO_x^{-1305\ cm^{-1}}{}_{(ads)}$, $NO_{ads}^{1580\ cm^{-1}}$, and "$HNO"_{(ads)}^{1540\ cm^{-1}}$ are shown

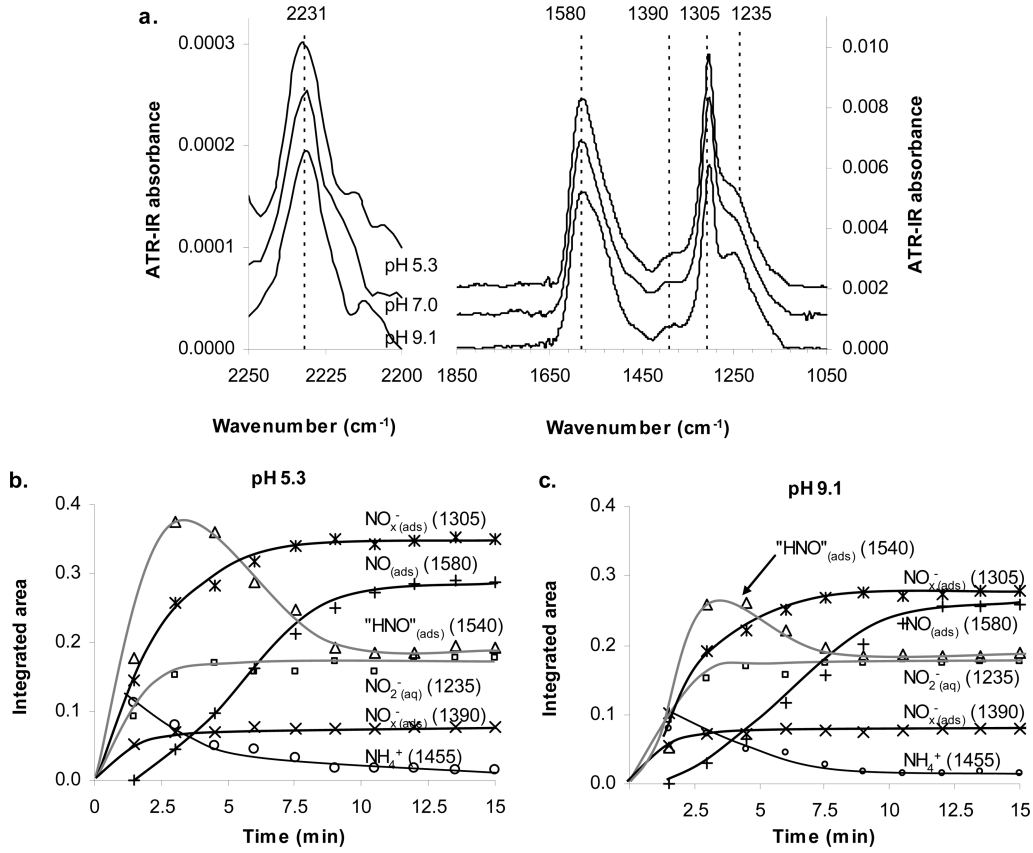

Figure 7. (a) Water corrected ATR-IR spectra after adsorption of $NO_2^-{}_{(aq)}$ on H−Pt/Al_2O_3 at pH 5.3, 7.0, and 9.1 for 15 min. Corresponding integrated peak areas at pH 5.3 (b) and pH 9.1 (c).

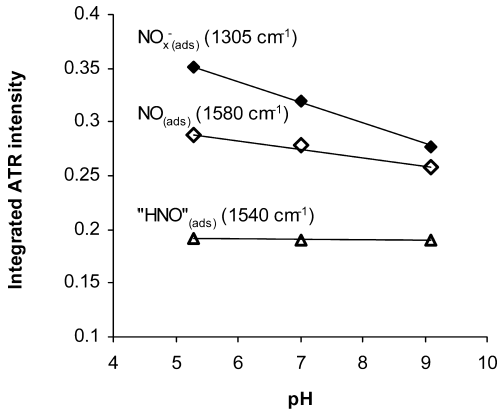

Figure 8. Integrated peak areas of a few adsorbed species as a function of pH, after adsorption of nitrite on H−Pt/Al_2O_3 for 15 min.

in Figure 8. Clearly, for $NO_x^-{}^{1305\ cm^{-1}}_{(ads)}$, the largest change in intensity is observed, about 20% lower at pH 9.1 compared to pH 5.3. For $NO_{ads}^{1580\ cm^{-1}}$, the decrease was approximately 10% in the same pH interval.

Hydrogenation of $NO_x^-{}_{(ads)}$, "HNO"$_{(ads)}$, and NO_{ads} on Pt/Al_2O_3. After $NO_2^-{}_{(aq)}$ adsorption on H−Pt/Al_2O_3, the cell was flushed with Ar/H_2O at the same pH as applied for adsorption. During flushing, the peaks of "HNO"$_{(ads)}$ and $NO_{(ads)}$ decreased slightly and a slight increase was observed for $NO_{ads}^{1580\ cm^{-1}}$, similar to our previous studies.[3] Further, $NO_2^-{}_{(aq)}$ was flushed out of the cell entirely, whereas N_2O was observed all the time, as it is continuously formed from "HNO"$_{(ads)}$ and $NO_{(ads)}$, in agreement with the small decrease in intensity for these two species.[3] Subsequently, H_2/H_2O was introduced to hydrogenate the adsorbed species. Figure 9 shows the ATR-IR spectra at pH 5.3 and the corresponding integrated peak areas during hydrogenation.

The patterns observed in Figure 9 are similar to those observed at pH 7.0 and discussed in a previous publication.[3] In summary, initially $NO_{steps}^{1620\ cm^{-1}}$ decreased in intensity while "HNO"$^{1540\ cm^{-1}}_{(ads)}$ increased. Simultaneously, $NO_x^-{}^{1305\ cm^{-1}}_{(ads)}$ decreased while $NO_{steps}^{1620\ cm^{-1}}$ appeared. The peak at 1620 cm^{-1} was assigned to NO adsorbed on isolated step sites on the basis of its stability and the absence of dipole−dipole interactions. Subsequently, the intensity of "HNO"$^{1540\ cm^{-1}}_{(ads)}$ decreased with a simultaneous increase in intensity of $NH_4^{+\ 455\ cm^{-1}}$. Further, $HNO_2^-{}^{1270\ cm^{-1}}_{(ads)}$ developed as an asymmetric peak at 1270 cm^{-1}, which only slightly decreased during H_2/H_2O flow (−10%).

Figure 10 shows the integrated intensity of "HNO"$^{1540\ cm^{-1}}_{(ads)}$, $HNO_2^-{}^{1270\ cm^{-1}}_{(ads)}$, $NO_{steps}^{1620\ cm^{-1}}$, and $NO_{ads}^{1580\ cm^{-1}}$ at different pH values as a function of time. The following trends are observed:

- The maximum intensities of "HNO"$^{1540\ cm^{-1}}_{(ads)}$ and $NO_{steps}^{1620\ cm^{-1}}$ vary with pH: $I_{pH\ 5.3} > I_{pH\ 7.0} > I_{pH\ 9.1}$.
- "HNO"$^{1540\ cm^{-1}}_{(ads)}$ disappears the fastest at low pH despite its higher maximal intensity during the experiment.
- Initially, the rate of development and the integrated intensity of $HNO_2^-{}^{1270\ cm^{-1}}_{(ads)}$ depends only slightly on pH. The final intensity is independent of pH.
- Initially, $NO_{ads}^{1580\ cm^{-1}}$ disappears faster at pH 5.3, but the total time of removal is independent of pH.

Discussion

Adsorption of $NO_2^-{}_{(aq)}$ on Pt/Al_2O_3 and Pd/Al_2O_3. Adsorption of $NO_2^-{}_{(aq)}$ on Pd/Al_2O_3 (Figure 1) and Pt/Al_2O_3 (Figure 6) reveals that the type of surface species observed on each catalyst are independent of pH, since the frequencies of the infrared peaks do not change. For both catalysts, the peaks have

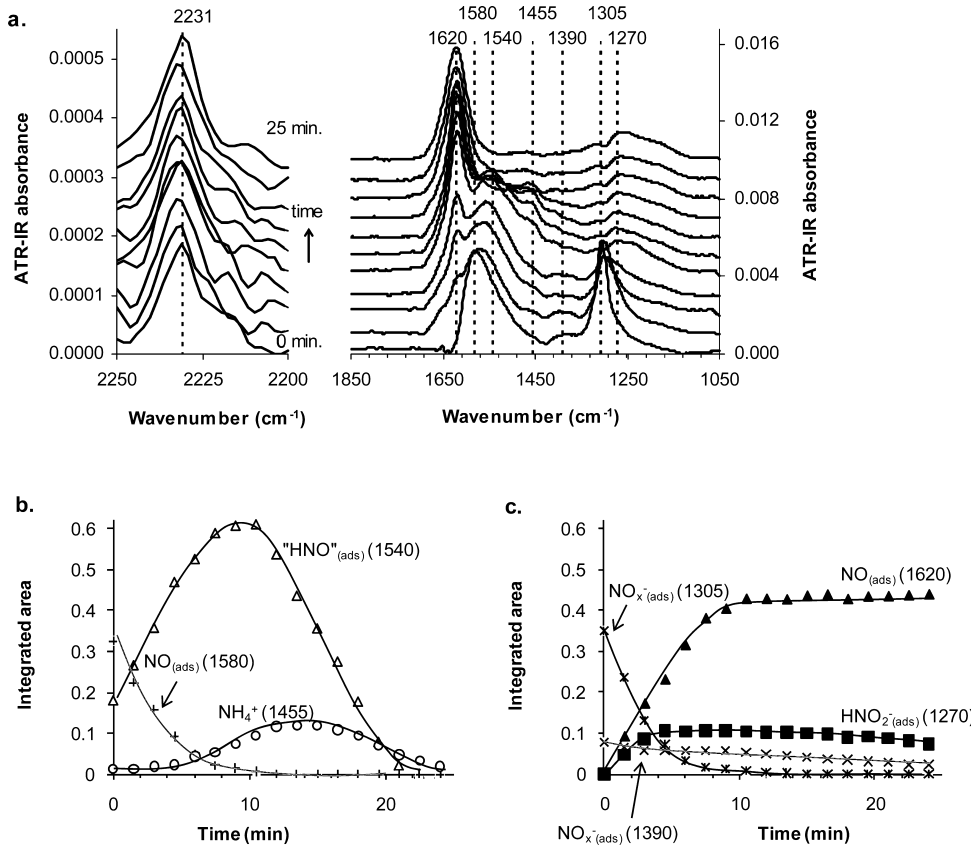

Figure 9. (a) Water corrected ATR-IR spectra during hydrogenation of $NO_x^-{}_{(ads)}$, $NO_{(ads)}$, "HNO"$_{(ads)}$, and $NO_x^-{}_{(ads)}$ on Pt/Al_2O_3, formed on the catalyst surface during adsorption of $NO_2^-{}_{(aq)}$ on $H-Pt/Al_2O_3$ at pH 5.3. (b and c) Corresponding integrated peak intensities during hydrogenation.

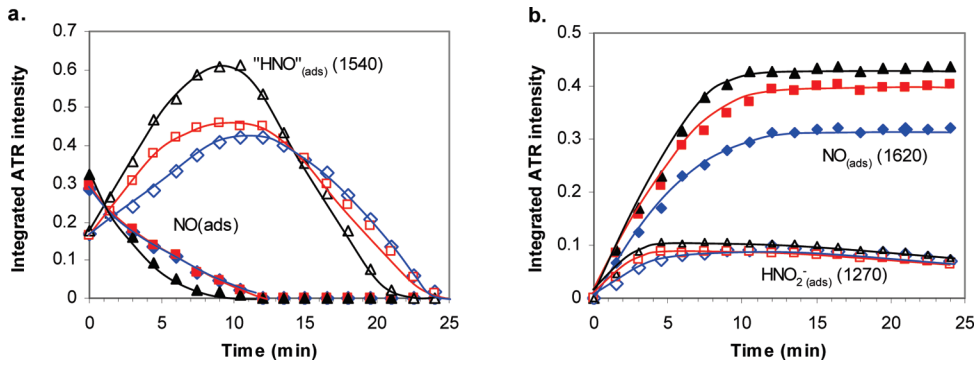

Figure 10. Time related integrated intensities of adsorbed species on Pt/Al_2O_3 during the hydrogenation as a function of pH. pH 5.3: black ▲, △; pH 7.0: red ■, □; pH 9.1: blue ◆, ◇. (a) Closed symbols, $NO_{ads}^{1580\ cm^{-1}}$; open symbols, "HNO"$_{(ads)}^{1540\ cm^{-1}}$. (b) Closed symbols, $HNO_2^-{}_{(ads)}^{1270\ cm^{-1}}$; open symbols, $NO_{steps}^{1620\ cm^{-1}}$.

been assigned to $NO_x^-{}_{(ads,\,x=2,3)}$ adsorbed on the metal particles.[3,10] On the other hand, the peak intensity is clearly different; higher amounts of NO_2^- adsorbed at lower pH. Since the intensity of $NO_2^-{}_{(aq)}$ (1235 cm^{-1}) is constant within the experimental error for both Pd/Al_2O_3 and Pt/Al_2O_3, neither the extinction coefficient nor the penetration depth of the evanescence wave are influenced by pH. Decreasing pH results in more positively charged metal particles, which promotes adsorption of anions by electrostatic forces.[29] Consequently, lower pH promotes adsorption of NO_2^-, as is observed in our experiments. These results are in good agreement with adsorption of NO_2^- on Pd/C, where higher amounts of adsorbed NO_2^- on Pd/C were found at lower pH.[30] On Pt/Al_2O_3, the intensities of $NO_x^-{}_{(ads)}^{1305\ cm^{-1}}$ and $NO_x^-{}_{(ads)}^{1390\ cm^{-1}}$ decrease similarly with higher pH (Figure 6). On Pd/Al_2O_3, however, the amount of $NO_x^-{}_{(ads)}^{1405\ cm^{-1}}$ decreases much more with increasing pH than the amount of $NO_x^-{}_{(ads)}^{1325\ cm^{-1}}$, confirming the assignment of these two peaks to differently adsorbed $NO_x^-{}_{(ads)}$ species as previously discussed.[10]

Adsorption and Hydrogenation of $NO_2^-{}_{(aq)}$ on $H-Pt/Al_2O_3$. The adsorbed species detected during adsorption of $NO_2^-{}_{(aq)}$ on $H-Pt/Al_2O_3$ at pH 5.3−9.1 (Figure 7) are identical to the species reported previously at neutral pH, namely, $NO_x^-{}_{(ads)}^{1305\ cm^{-1}}$, $NO_x^-{}_{(ads)}^{1390\ cm^{-1}}$, "HNO"$_{(ads)}^{1540\ cm^{-1}}$, and $NO_{ads}^{1580\ cm^{-1}}$.[3] In addition, $NH_4^+{}^{1455\ cm^{-1}}$ and N_2O (2231 cm^{-1}) were also detected. The patterns of evolution of adsorbed species are similar at all pH values investigated, but the final intensity of the species depends on pH (Figure 8). The integrated intensity of $NO_x^-{}_{(ads)}^{1305\ cm^{-1}}$ decreases with higher pH, similar to the result on passivated Pt/Al_2O_3, but the amount of $NO_x^-{}_{(ads)}^{1390\ cm^{-1}}$ is independent of pH when adsorbed on $H-Pt/Al_2O_3$. At present, we do not have an explanation for the constant signal of $NO_x^-{}_{(ads)}^{1390\ cm^{-1}}$. Moreover, it should be realized that the intensities of $NO_x^-{}_{(ads)}^{1305\ cm^{-1}}$ and

$NO_x^{-}{}_{(ads)}^{1390\ cm^{-1}}$ on H−Pt/Al_2O_3 are much lower than those after adsorption on oxygen covered Pt/Al_2O_3 (Figure 6), and in addition, many more surface species are present after adsorption of nitrite on H−Pt/Al_2O_3 which could induce local effects on the surface of the metal particles.

Figure 8 also shows that the final intensity of "HNO"$_{(ads)}^{1540\ cm^{-1}}$ does not depend on pH, while the intensity of $NO_{ads}^{1580\ cm^{-1}}$ decreases at higher pH. As a result, the $NO_{ads}^{1580\ cm^{-1}}$/"HNO"$_{(ads)}^{1540\ cm^{-1}}$ ratio decreases with increasing pH. Further, the development of "HNO"$_{(ads)}^{1540\ cm^{-1}}$ with time is clearly affected by pH, as can be seen in Figure 7: the maximum intensity of "HNO"$_{(ads)}^{1540\ cm^{-1}}$ is about 1.5 times higher at pH 5.3 compared to pH 9.1. As shown in Scheme 1, on H−Pt/Al_2O_3, both $NO_{ads}^{1580\ cm^{-1}}$ and "HNO"$_{(ads)}^{1540\ cm^{-1}}$ are intermediates in the reactions toward N_2O and NH_4^+. The development of their respective intensities with time is thus the result of the balance between reaction rates of formation and reaction rates to the subsequent products. Obviously, during the adsorption of nitrite on H−Pt/Al_2O_3, the pH affects individual rates of intermediate steps in such a way that the amount of adsorbed species at the end of the adsorption is different for each pH.

The subsequent hydrogenation of the adsorbed species on H−Pt/Al_2O_3 is also affected by pH (Figures 9 and 10). The effects are most pronounced for the formation of $NO_{steps}^{1620\ cm^{-1}}$ and the formation and disappearance of "HNO"$_{(ads)}^{1540\ cm^{-1}}$. It was shown before that $NO_{steps}^{1620\ cm^{-1}}$only develops if H_2 is abundantly available and $NO_{steps}^{1620\ cm^{-1}}$only very slowly removes from the platinum surface.[3] The different intensity of $NO_{steps}^{1620\ cm^{-1}}$ thus reflects a different rate of formation with pH. For the removal of "HNO"$_{(ads)}^{1540\ cm^{-1}}$, the situation is more complicated, since the observed intensity results from the balance between the rate of formation and the rates of reaction to various products (Scheme 1). After approximately 12 min, only the intensities of "HNO"$_{(ads)}^{1540\ cm^{-1}}$ and $NH_4^{+}\ ^{1455\ cm^{-1}}$ change significantly, with the other species being removed or having a constant intensity. Figure 10 shows that after 12 min the rate of removal of "HNO"$_{(ads)}^{1540\ cm^{-1}}$ is faster at lower pH, even when the same coverage is reached as at other pH values. This observation seems to be in good agreement with the literature, reporting faster nitrite hydrogenation at lower pH in batch reactors.[13,31,32] There is, however, no simple explanation for the increased rate at lower pH because of the complicated intertwined reaction scheme for nitrite hydrogenation over H−Pt/Al_2O_3 (Scheme 1).

Finally, during adsorption of $NO_2^{-}{}_{(aq)}$ on H−Pt/Al_2O_3 and its subsequent hydrogenation, the peak intensity for N_2O was very low and remained constant at all times. N_2O is not strongly adsorbed on platinum surfaces[33] and can easily be flushed out of the cell.[3] Since the exact mechanism for N_2O formation is unclear and the hydrogenation pathways are entangled for H−Pt/Al_2O_3 (Scheme 1), the present ATR results do not allow for conclusive statements on the exact effect of pH on the NH_4^+/N_2O selectivity for H−Pt/Al_2O_3. Additional studies are required in which steady state experiments are performed at different pHs and different H_2 concentrations. Moreover, steady state isotopic transient kinetic analysis (SSITKA) could be applied to separate the different pathways to the respective products.

Adsorption and Hydrogenation of $NO_2^{-}{}_{(aq)}$ on H−Pd/Al_2O_3. At pH values ranging from 6.0 to 9.1, adsorption of $NO_2^{-}{}_{(aq)}$ on H−Pd/Al_2O_3 leads to the same adsorbed species on the palladium surface, namely, $NO_{(ads)}^{1720\ cm^{-1}}$, $NH_{2(ads)}^{1510\ cm^{-1}}$, and $NH_4^{+}\ ^{1450\ cm^{-1}}$ (Figure 2). In addition, only at pH 5.1, $NO_x^{-}{}_{(ads)}$ was observed on the catalyst (1405 and 1325 cm^{-1}), but the amount was only 10% of the amount observed after adsorption on passivated Pd/Al_2O_3 (Figure 1). The presence of adsorbed nitrite at lower pH is similar to observation on H−Pt/Al_2O_3 and can be likewise attributed to a higher positive surface charge of the palladium particles at lower pH.

Figure 3 shows opposite behavior of the integrated intensity of $NO_{(ads)}^{1720\ cm^{-1}}$ and $NH_{2(ads)}^{1510\ cm^{-1}}$ as a function of pH: $NO_{(ads)}^{1720\ cm^{-1}}$ decreases and $NH_{2(ads)}^{1510\ cm^{-1}}$ increases with increasing pH. In addition, the exact peak position of $NO_{(ads)}^{1720\ cm^{-1}}$ shifts from 1723 to finally 1717 cm^{-1} with increasing pH. The shifts are small but reproducible and consistent with the lower intensity at higher pH. Both the shift and the lower intensity point to a lower surface coverage of $NO_{(ads)}^{1720\ cm^{-1}}$ at higher pH, since the peak position of this NO species is dependent on its surface coverage *via* a dipole−dipole interaction. Similar to H−Pt/Al_2O_3, the observed intensities for $NO_{(ads)}^{1720\ cm^{-1}}$ and $NH_{2(ads)}^{1510\ cm^{-1}}$are the combined result of the rates of formation and consecutive rates of reaction to products when adsorbing nitrite on H−Pd/Al_2O_3 (Scheme 1). Interestingly, the $NO_{(ads)}^{1720\ cm^{-1}}$/$NH_{2(ads)}^{1510\ cm^{-1}}$ ratio shows the same trend with pH as observed in continuous nitrite hydrogenation experiments with increasing H_2 concentration.[10,34]

In addition to the adsorption, subsequent hydrogenation of the adsorbed species on H−Pd/Al_2O_3 varies with pH (Figure 5). For $NO_{(ads)}^{1720\ cm^{-1}}$, the time required for complete hydrogenation is almost the same in the range of pH investigated (Figure 5a). However, as discussed above, the surface coverage of $NO_{(ads)}^{1720\ cm^{-1}}$ is much higher at lower pH; thus, the rate of $NO_{(ads)}^{1720\ cm^{-1}}$ hydrogenation decreases with pH in the order: pH 5.1 > pH 6.0 > pH 7.8 > pH 9.1. The increased rate cannot only be attributed to the higher initial coverage, when at pH 5.1 the same intensity is reached as the initial intensity of $NO_{(ads)}^{1720\ cm^{-1}}$ at pH 9.1 (after approximately 10 min), the remaining amount at pH 5.1 is removed about twice as fast as at pH 9.1. Thus, it can be concluded that the rate constant $k_{NO\rightarrow N_2}$ increases with decreasing pH.

In contrast, hydrogenation of $NH_{2(ads)}^{1510\ cm^{-1}}$ is the fastest at high pH (Figure 5b): starting with the highest initial intensity, the time required for complete removal is the shortest, leading to increasing hydrogenation rates in the order pH 5.1 < pH 6.0 < pH 7.8 < pH 9.1. In this case, the average rate of removal at pH 5.1 is approximately 3 times slower than that at pH 9.1. Again, the increased rate cannot only be attributed to the higher initial coverage, because at equal coverage (after about 18 min) still $NH_{2(ads)}^{1510\ cm^{-1}}$ disappears the slowest at pH 5.1 and the fastest at pH 9.1. As a consequence, $k_{NH_2\rightarrow NH_4^+}$ decreases with decreasing pH. These results are in agreement with publications on the selectivity toward ammonia which has been reported to increase with increasing pH as well as with higher H_2 concentration.[2,4,5,7,11,31,34]

Moreover, the adsorption experiments at different pHs (Figures 2 and 3) show that, despite the increased rates of reaction for $NO_{(ads)}^{1720\ cm^{-1}}$at low pH and for $NH_{2(ads)}^{1510\ cm^{-1}}$at high pH, also the amounts after adsorption are high for the respective adsorbates. This leads to the conclusion that rates of formation of $NO_{(ads)}^{1720\ cm^{-1}}$at low pH ($r_{NO_2^-\rightarrow NO}$) and $NH_{2(ads)}^{1510\ cm^{-1}}$at high pH ($r_{NO_2^-\rightarrow NH_2}$) are even more increased than their respective rates of consecutive reaction. Similarly, we have shown that CO adsorption and subsequent oxidation in water on Pt/Al_2O_3 and Pd/Al_2O_3 also depend on pH.[25,35,36] The observed increased CO oxidation rate at higher pH was attributed to a change in metal particle potential induced by pH. The currently observed phenomena for nitrite adsorption and hydrogenation could be related to the metal particle potential as well. This will be investigated more closely by ATR-IR spectroscopy during steady state experiments and additional transient experiments at different pHs and H_2 concentrations.

Considering the proposed reaction pathway for H−Pd/Al_2O_3 as depicted in Scheme 1, it can be concluded that the scheme should be extended by adding the observation of adsorbed nitrite species at low pH. However, unlike Pt/Al_2O_3, it is not clear how (or which of) the nitrite species are specifically attributing to one of the independent pathways over Pd/Al_2O_3. In agreement with a recent study, the experimental data in Figure 4 show that $NO_{(ads)}^{1720\ cm^{-1}}$ is hydrogenated to a species which is not infrared active, most likely N_2.[10] In contrast to Pt/Al_2O_3, N_2O was not observed on Pd/Al_2O_3 during hydrogenation of $NO_{(ads)}$. The absence of N_2O, however, is probably due to fast reduction of N_2O to N_2 over palladium catalysts, as reported in the literature.[37]

In essence, this ATR-IR spectroscopy study convincingly shows that the change in selectivity with pH observed during nitrite hydrogenation over palladium catalysts in batch reactors can be attributed to changes in individual rate constants for the formation and hydrogenation of $NO_{(ads)}^{1720\ cm^{-1}}$ and $NH_{2(ads)}^{1510\ cm^{-1}}$. On H−Pd/$Al_2O_3$, $k_{NO\rightarrow N_2}$ decreases and $k_{NH_2\rightarrow NH_4^+}$ increases with rising pH values, thus both increasing the selectivity toward ammonia at higher pH. On the basis of the present results for H−Pt/Al_2O_3, no conclusions can be drawn about selectivity because of the entangled reaction paths, but clearly the total hydrogenation activity increased with decreasing pH.

Conclusion

ATR-IR spectroscopy proved to be a valuable tool for a detailed investigation on surface intermediates during nitrite hydrogenation in water over noble metal catalysts. On both Pd/Al_2O_3 and Pt/Al_2O_3, a clear influence of pH is observed on adsorption and subsequent hydrogenation of nitrite in water. For Pt/Al_2O_3, larger amounts and faster hydrogenation rates were found at lower pH for reaction intermediates like $NO_{steps}^{1620\ cm^{-1}}$ and "HNO"$_{(ads)}^{1540\ cm^{-1}}$, explaining the higher TOF at lower pH as reported in the literature. For Pd/Al_2O_3, it can be concluded that the effect of pH on selectivity is controlled by the rate constants of formation and subsequent hydrogenation of the most stable reaction intermediates to N_2 ($NO_{(ads)}$) and NH_4^+ ($NH_{2(ads)}$), respectively. The rate constant of $NO_{(ads)}$ hydrogenation decreases whereas the rate constant of $NH_{2(ads)}$ hydrogenation increases with increasing pH. The origin of the pH effect on the rate constants might be due to an alteration of the metal particle potential, which will be the subject of future investigations.

Acknowledgment. This work was financially supported by DSM Research, The Netherlands. This work was performed under the auspices of The Dutch Institute for Research in Catalysis (NIOK). We thank Ing. Bert Geerdink for technical support.

References and Notes

(1) World Health Organization, Water and health in Europe, WHO, Regional Office for Europe, Copenhagen, 2002.
(2) Vorlop, K. D.; Tacke, T. *Chem. Ing. Tech.* **1989**, *61*, 836–837.
(3) Ebbesen, S. D.; Mojet, B. L.; Lefferts, L. *J. Phys. Chem. C* **2009**, *113* (6), 2503–2511.
(4) Deganello, F.; Liotta, L. F.; Macaluso, A.; Menezia, A. M.; Deganello, G. *Appl. Catal., B* **2000**, *24*, 265–273.
(5) Matatov-Meytal, Y.; Barelko, V.; Yuranov, I.; Kiwi-Minsker, L.; Renken, A.; Sheintuch, M. *Appl. Catal., B* **2001**, *31*, 233–240.
(6) Hörold, S.; Vorlop, K. D.; Tacke, T.; Sell, M. *Catal. Today* **1993**, *17*, 21–30.
(7) Prüsse, U.; Hahnlein, M.; Daum, J.; Vorlop, K. D. *Catal. Today* **2000**, *55*, 79–90.
(8) Wärnå, J.; Turunen, I.; Salmi, T.; Maunula, T. *Chem. Eng. Sci.* **1994**, *49*, 5763–5773.
(9) Hörold, S.; Tacke, T.; Vorlop, K. D. *Environ. Technol.* **1993**, *14*, 931–939.
(10) Ebbesen, S. D.; Mojet, B. L.; Lefferts, L. *J. Catal.* **2008**, *256*, 15–23.
(11) Pintar, A.; Setinc, M.; Levec, J. *J. Catal.* **1998**, *174*, 72–87.
(12) Ebbesen, S. D.; Mojet, B. L.; Lefferts, L. *Langmuir* **2008**, *24*, 869–879.
(13) Prüsse, U.; Daum, J.; Bock, C.; Vorlop, K. D. *Stud. Surf. Sci. Catal.* **2000**, *130*, 2237–2242.
(14) Pintar, A.; Batista, J.; Levec, J. *Water Sci. Technol.* **1998**, *37*, 177–185.
(15) Matatov-Meytal, Y.; Barelko, V.; Yuranov, I.; Sheintuch, M. *Appl. Catal., B* **2000**, *27*, 127–135.
(16) Matatov-Meytal, Y.; Shindler, Y.; Sheintuch, M. *Appl. Catal., B* **2003**, *45*, 127–134.
(17) Ebbesen, S. D. Spectroscopy under the Surface - In-Situ ATR-IR Studies of Heterogeneous Catalysis in Water. Doctoral Thesis, University of Twente, Enschede, The Netherlands, 2007.
(18) Balbaud, F.; Sanchez, G.; Santarini, G.; Picard, G. *Eur. J. Inorg. Chem.* **2000**, *4*, 665–674.
(19) Gootzen, J. F. E.; van Hardeveld, R. M.; Visscher, W.; van Santen, R. A.; van Veen, J. A. R. *Recl. Trav. Chim. Pays-Bas* **1996**, *115*, 480–485.
(20) Nishimura, K.; Machida, K.; Enyo, M. *Electrochim. Acta* **1991**, *36*, 877–880.
(21) Rodes, A.; Gomez, R.; Orts, J. M.; Feliu, J. M.; Aldaz, A. *J. Electroanal. Chem.* **1993**, *359*, 315–323.
(22) Rosca, V.; Koper, M. T. M. *Surf. Sci.* **2005**, *584*, 258–268.
(23) Ye, S.; Kita, H. *J. Electroanal. Chem.* **1993**, *346*, 489–495.
(24) Dima, G. E.; Beltramo, G. L.; Koper, M. T. M. *Electrochim. Acta* **2005**, *50*, 4318–4327.
(25) Mojet, B. L.; Ebbesen, S. D.; Lefferts, L. *Chem. Soc. Rev.*, DOI: 10.1039/C0CS00014K.
(26) *CRC Handbook of chemistry and physics*, 90th ed. online; CRC Press: Boca Raton, Florida 2009−2010.
(27) Ebbesen, S. D.; Mojet, B. L.; Lefferts, L. *Langmuir* **2006**, *22*, 1079–1085.
(28) Hadjiivanov, K. I. *Catal. Rev.—Sci. Eng.* **2000**, *42*, 71–144.
(29) Couto, A.; Rincón, A.; Pérez, M. C.; Gutiérrez, C. *Electrochim. Acta* **2001**, *46*, 1285–1296.
(30) Mikami, I.; Sakamoto, Y.; Yoshinaga, Y.; Okuhara, T. *Appl. Catal., B* **2003**, *44*, 79–86.
(31) Tacke, T.; Vorlop, K. D. *Chem. Ing. Tech.* **1993**, *65*, 1500–1502.
(32) Prüsse, U.; Morawsky, V.; Dierich, A.; Vaccaro, A.; Vorlop, K.-D. *Prep. Catal. VII, Stud. Surf. Sci. Catal.* **1998**, *118*, 137–146.
(33) Avery, N. R. *Surf. Sci.* **1983**, *131*, 501–510.
(34) Chinthaginjala, J. K.; Lefferts, L. *Appl. Catal., B*, submitted for publication, **2010**.
(35) Ebbesen, S. D.; Mojet, B. L.; Lefferts, L. *Phys. Chem. Chem. Phys.* **2009**, *11*, 641–649.
(36) Ebbesen, S. D.; Mojet, B. L.; Lefferts, L. *J. Catal.* **2007**, *246*, 66–73.
(37) de Vooys, A. C. A.; Koper, M. T. M.; van Santen, R. A.; van Veen, J. A. R. *J. Catal.* **2001**, *202*, 387–394.

JP106521T